energies

MDPI

Article

A Novel Sooty Terns Algorithm for Deregulated MPC-LFC Installed in Multi-Interconnected System with Renewable Energy Plants

Hossam Hassan Ali [1], Ahmed Fathy [2], Abdullah M. Al-Shaalan [3], Ahmed M. Kassem [4], Hassan M. H. Farh [3,*], Abdullrahman A. Al-Shamma'a [3] and Hossam A. Gabbar [5]

1 Electrical Department, Faculty of Technology and Education, Sohag University, Sohag 82524, Egypt; hossam_hassan123@techedu.sohag.edu.eg
2 Electrical Power & Machine Department, Faculty of Engineering, Zagazig University, Zagazig 44519, Egypt; elmohandes.ahmed@gmail.com
3 Electrical Engineering Department, College of Engineering, King Saud University, Riyadh 11421, Saudi Arabia; shaalan@ksu.edu.sa (A.M.A.-S.); ashammaa@ksu.edu.sa (A.A.A.-S.)
4 Electrical Engineering Department, Faculty of Engineering, Sohag University, Sohag 82524, Egypt; ahmed.kassem@eng.sohag.edu.eg
5 Faculty of Energy Systems and Nuclear Science, Ontario Tech University (UOIT), 2000 Simcoe St N, Oshawa, ON L1G 0C5, Canada; hossam.gaber@ontariotechu.ca
* Correspondence: hfarh1@ksu.edu.sa

Abstract: This paper introduces a novel metaheuristic approach of sooty terns optimization algorithm (STOA) to determine the optimum parameters of model predictive control (MPC)-based deregulated load frequency control (LFC). The system structure consists of three interconnected plants with nonlinear multisources comprising wind turbine, photovoltaic model with maximum power point tracker, and superconducting magnetic energy storage under deregulated environment. The proposed objective function is the integral time absolute error (ITAE) of the deviations in frequencies and powers in tie-lines. The analysis aims at determining the optimum parameters of MPC via STOA such that ITAE is minimized. Moreover, the proposed STOA-MPC is examined under variation of the system parameters and random load disturbance. The time responses and performance specifications of the proposed STOA-MPC are compared to those obtained with MPC optimized via differential evolution, intelligent water drops algorithm, stain bower braid algorithm, and firefly algorithm. Furthermore, a practical case study of interconnected system comprising the Kuraymat solar thermal power station is analyzed based on actual recorded solar radiation. The obtained results via the proposed STOA-MPC-based deregulated LFC confirmed the competence and robustness of the designed controller compared to the other algorithms.

Keywords: deregulated LFC; renewable energy; model predictive control; sooty terns optimization

Citation: Ali, H.H.; Fathy, A.; Al-Shaalan, A.M.; Kassem, A.M.; M. H. Farh, H.; Al-Shamma'a, A.A.; A. Gabbar, H. A Novel Sooty Terns Algorithm for Deregulated MPC-LFC Installed in Multi-Interconnected System with Renewable Energy Plants. *Energies* **2021**, *14*, 5393. https://doi.org/10.3390/en14175393

Academic Editor: Antonio Rosato

Received: 29 July 2021
Accepted: 21 August 2021
Published: 30 August 2021

1. Introduction

In the interconnected system, the frequency stabilization is very significant to keep the stability of the power system which is achieved by load frequency control (LFC). LFC aims at keeping the frequency at nominal value and vanishing the aberration in frequency and power flow in tie-lines to zero in case of sudden load disturbance. The objective of interconnecting multiplants is to share loads and maintain the system dependability in the event of curtailment of any generation plant. Recently, renewable energy sources (RESs) have been combined with conventional plants and installed in electric grids [1–3]. The deregulated power system is a conventional power system with modified structure. It consists of many autonomous entities such as transmission companies (TRANSCOs), distribution companies (*DISCOs*), and generation companies (*GENCOs*). The *GENCOs*, as autonomous power units, may contribute in the LFC task. Moreover, *DISCOs* may contract unilaterally

with *GENCOs*, nonconventional power source units, or independent power producers (IPPs) in different areas. In the deregulated system, control is highly decentralized and independent system operators (ISOs) are responsible for keeping the steady frequency and tie-line power flow within their acceptable limits [4,5]. The deregulated LFC is presented in many reported works with optimal control techniques. In [6], fuzzy proportional-integral-derivative (F-PID) was optimized via mine blast algorithm (MBA), and the presented controller was designed with five memberships. RESs and flexible alternating current transmission (FACT) are installed in the interconnected power system to minimize overshoot and settling time. Sine cosine algorithm is used to adapt cascade control fractional order (FO), integral FO (FOI), and proportional-derivative (FOPD) such that it minimizes the integral square error (ISE) [7]. Deregulated LFC with installed thyristor-controlled phase shifter (TCPS) and superconducting magnetic energy source (SMES) have been presented with the aid of adaptive neuro Fuzzy system (ANFIS) to improve the dynamic response of the system [8]. Improved particle swarm optimization (IPSO) has been presented to optimize tilted integral derivative (TID) and FOPID-based deregulated LFC installed with static synchronous series compensator (SSSC), the considered fitness function to be minimized was the integral time square error (ITSE) [9]. Deregulated LFC has been presented with incorporating dish-Stirling solar thermal system (DSTS), geothermal power plant (GTPP), and high-voltage direct current (HVDC)-based cascade FOPI-FOPID optimized via sin cosine algorithm (SCA) [10]. TID control has been adapted by hybrid teaching learning-based optimizer and pattern search (hTLBO-PS) with SMES and TCPS; the employed fitness function in that work was ISE [11]. Fuzzy-PID-LFC controller has been determined through bacterial foraging optimization algorithm (BFOA) for multisources interconnected systems [12]. Sliding mode control (SMC)-based output feedback has been employed to optimize LFC installed in multi-sources interconnected system, the target is to minimize the ISE via hybrid flower pollination and pattern search (hFPA-PS) [13]. In [14], cascade tilt-integral–TID (C-TI-TID) was presented to optimize deregulated LFC installed in four areas via water cycle algorithm (WCA), and the results were compared with C-PI-TD. Redox flow battery (RFB) was introduced to minimize the peak overshoot and settling time of the frequency and tie-line power responses for multi-interconnected system with multisources with LFC, using predictive functional modified PID (PFMPID) adjusted via grasshopper optimization algorithm (GOA); seven membership functions were employed to design the fuzzy controller [15]. In [16], the volleyball premier league algorithm (VPL) was presented to optimize cascade structure of a two-degree-of-freedom PI and FOPD controller with filter incorporated with HVDC and distributed generation (DG) in deregulated LFC. A quasi-oppositional harmony search algorithm (QOHS) has been introduced to optimize deregulated LFC with Sugeno fuzzy-PID with three membership functions-integrated thyristor-controlled series compensator (TCSC); ISE was selected as the target [17–19]. In [20], PID with double-derivative (PIDD)-based deregulated LFC with integrated HVDC was introduced and optimized via fruit fly optimization algorithm (FOA). A cascade PID with filter (PIDF) and one plus FO derivative (1+FOD) were employed to simulate LFC with HVDC and SSSC, and the controller was optimized via salp swarm algorithm (SSA) [21]. In [22], FOA was introduced to tune a PID controller with filter incorporated in a deregulated LFC-based unified power flow controller (UPFC) and HVDC. In [23], a PI controller was presented in a deregulated LFC installed with multisources and capacitive energy storage (CES) optimized via SCA. A modified virus colony search (MVCS) was studied to optimize PID controller-based deregulated LFC installed in four interconnected areas [24]. A PID controller was optimized via artificial cooperative search algorithm (ACSA)-based deregulated LFC with combined RFB and SMES [25]. A bat algorithm was presented to optimize FOPID-based deregulated LFC with incorporated SMES and UPFC to minimize ITAE [26].

Recently, there are some new approaches applied to simulate the deregulated LFC, such as SSA [27,28], crow search algorithm (CA) [29], the whale optimization [30], GOA [31], MBA [32], opposition-based interactive search algorithm (OISA) [33], and quasi-opposition

lion optimization algorithm (QOLOA) [34]). Table 1 presents comparison of previous studies reported in deregulated LFC on the basis of control type, optimization approach, and system construction. Moreover, comparison of the reported approaches that have been conducted in LFC in three areas with multisources deregulated is given in Table 2.

Regarding the reported works and the comparisons given in Tables 1 and 2, one can see that few researchers considered deregulated multi-interconnected systems including optimal MPC and RESs. Moreover, the application of metaheuristic approaches in this field is still limited. Furthermore, the traditional controllers reported in many previous works failed in vanishing the fluctuations in frequencies and tie-line powers for interconnected systems when nonlinearities of system are considered. Additionally, most of the metaheuristic approaches used in that field may trap in local optima.

The authors covered these defects by proposing a novel methodology incorporated the sooty terns optimization algorithm (STOA) to design the model-predictive control (MPC)-based LFC installed in multi-interconnected plants. The parameters of MPC are identified via STOA such that ITAE of aberrations in frequencies and powers in tie-lines is minimized. The contribution of this work is summarized as follows:

- A novel STOA approach is proposed to compute the MPC optimum parameters-based nonlinear deregulated LFC combined with conventional, RESs, and energy storage systems (ESSs).
- Wind turbine (WT), photovoltaic (PV) model with maximum power point tracker (MPPT), hydropower, diesel generator, and thermal plant are presented and modeled in deregulated LFC.
- Practical case study of interconnected system comprising the Kuraymat solar thermal power station is analyzed based on actual recorded solar radiation.
- The proposed MPC-LFC optimized via STOA achieved robust performance under changing some parameters of the system and random load disturbance.

The paper is organized as follows: Section 2 introduces the mathematical model of the deregulated LFC, Section 3 presents the proposed methodology, Section 4 presents simulation results, and Section 5 introduces conclusions.

Table 1. Comparison of reported works conducted in deregulated LFC.

Author	Year	Deregulated/ Conventional	Type of Controller	Optimization Approach	System Construction	Has RESs?/Type	Has ESs?/Type	Defects
Panwar, A. et al. [3]	2018	Conventional	PID	BFOA	2 areas	√ (Fuel cell)	×	– The deviation in frequency is large. – Weak performance in various operating conditions.
Shiva, C.K. et al. [17–19]	2016–2017	Deregulated	PID	QOHS	2, 3 and 5 areas, multisources	×	×	
Mohanty, B. et al. [20]	2015	Deregulated	PIDD	FOA	2-areas, multisources	×	×	
Dhundhara, S. et al. [23]	2018	Deregulated	PI	SCA	2 areas, multisources	×	√ (CES)	
Ghasemi-marzbali, A. [24]	2020	Deregulated	PID	MVCS	4 areas, multisources	×	×	
Selvaraju, R.K. et al. [25]	2016	Deregulated	PI	ACSA	2 areas, multisources	×	√ (SMES and RFB)	
Kumar, R. et al. [30]	2020	Deregulated	PI	Wahle algorithm	2 areas, multisources	×	√ (CES)	
Shankar, R. et al. [22]	2019	Deregulated	PID	FOA	2 areas, multisources	×	×	
Kumar, A. et al. [34]	2021	Deregulated	PIDN	QOLOA	2 areas, multisources	√ (WT and PV)	√ (SMES and RFB)	
Morsali, J. et al. [9]	2018	Deregulated	FOPID	MGSO	2 areas, multisources	×	×	– More consumption time. – To improve system dynamics, several parameters of control must be optimally tuned.
Prakash, A. et al. [21]	2020	Deregulated	PIDN(1+FOD)	SSA	2 areas, multisources	√ (WT)	×	
Mishra, D.K. et al. [26]	2020	Deregulated	FOPID	Bat Algorithm	2 areas, multisources	×	√ (SMES)	
Arya, Y. [2]	2019	Deregulated	FO-fuzzy PID	BFOA	2 and 3 areas, multisources	×	√ (RFB)	
Mishra, A.K. et al. [28]	2021	Deregulated	FO-fuzzy PID	SSA	3 areas, multisources	√ (WT, STPP and GTPP)	√ (RFB)	

Table 1. *Cont.*

Author	Year	Deregulated/ Conventional	Type of Controller	Optimization Approach	System Construction	Has RESs?/Type	Has ESs?/Type	Defects
Fathy, A. et al. [6]	2020	Conventional/ deregulated	Fuzzy PID	MBA	2 and 3 areas	×	×	– More consumption time due to fuzzy membership.
Arya, Y. et al. [12]	2017	Conventional/ deregulated	Fuzzy PI/PID	BFOA	2 area/2 areas, multisources	×	×	
Sharma, M. et al. [27]	2020	Deregulated	Fuzzy PIDN	SSA	2 areas, multisources	×	√ (RFB)	
Veerasamy, V. et al. [1]	2020	Conventional	Cascade PI-PD	PSO-GSA	2 areas, multisources	√ (WT, Fuel cell)	√ (Battery)	– Many controller parameters are required which increases the consumption time. – Selection of primary and secondary loops of controller is critical to achieve best system responses.
Tasnin, W. et al. [7]	2019	Deregulated	Cascade FOI-FOPD	SCA	3 areas, multisources	√ (WT, STPP and GTPP)	×	
Tasnin, W. et al. [10]	2018	Deregulated	Cascade FOPI-FOPID	SCA	2 areas, multisources	√ (DSTS and GTPP)	×	
Kumari, S. et al. [14]	2020	Deregulated	Calculus-based cascade TI-TID	WCA	4 areas, multisources	×	×	
Prakash, A. et al. [16]	2019	Deregulated	Cascade 2-DOF-PI-FOPDN	VPL	2 areas, multisources	×	×	
Babu, N.R. et al. [29]	2021	Deregulated	Cascade FOPDN-FOPIDN	CA	3 areas, multisources	√ (Realistic DSTS)	×	
Raj, U. et al. [33]	2020	Deregulated	Cascade 2DOF-PIDN-FOID	OISA	3 areas, multisources	√ (WT and PV)	×	
Pappachen, A. et al. [8]	2016	Deregulated	ANFIS	×	2 areas, multisources	×	√ (SMES)	– More complicated than other methods. – The parameters of controller have complete impact on the system dynamics.
Khamari, D. et al. [11]	2020	Deregulated	TID	hTLBO-PS	2 areas, multisources	√ (Solar thermal)	√ (SMES)	
Mohanty, B. [13]	2020	Deregulated	Output feedback SMC	hFPA-PS	2 areas, multisources	×	×	
Nosratabadi, S.M. et al. [15]	2019	Deregulated	Modified PID	GOA	3 areas, multisources	√ (WT)	√ (RFB)	
Das, M.K. et al. [31]	2021	Deregulated	PID-RLNN	GOA	3 areas, multisources	√ (WT)	√ (SMES)	
Das, S. et al. [32]	2021	Deregulated	TIDN-(1+PI)	MBA	3 areas, multisources	√ (WT, GTPP and wave energy)	×	
Present study		**Deregulated**	**Optimal MPC**	**STOA**	**3 areas, multisources**	**√ (WT, PV and STPP)**	**√ (SMES)**	

Table 2. Comparison of reported works conducted in three-areas with multi-sources deregulated LFC.

Author	Year	Type of Controller	Optimization Approach	Linear/ Nonlinear	Type of Generator	Has RESs?/Type	Cases Study					Has ESs?/Type
							1	2	3	4	5	
Arya, Y. [2]	2019	FO-fuzzy PID	BFOA	Linear	Thermal-hydro	×	√	√	×	×	×	√ (RFB)
Tasnin, W. et al. [7]	2019	Cascade FOI-FOPD	SCA	Linear	Thermal	√ (WT, STPP and GTPP)	√	√	√	×	×	×
Nosratabadi, S.M. et al. [15]	2019	Modified PID	GOA	Nonlinear (GRC-GDB)	Thermal-hydro-gas-diesel	√ (WT)	√	√	√	√	×	√ (RFB)
Shiva, C.K. et al. [17]	2016	PID	QOHS	Linear	Thermal	×	√	√	√	×	×	×
Mishra, A.K. et al. [28]	2021	FO-fuzzy PID	SSA	Nonlinear (GRC-GDB)	Thermal	√ (WT, STPP and GTPP)	√	√	√	√	×	√ (RFB)
Babu, N.R. et al. [29]	2021	Cascade FOPDN-FOPIDN	CA	Nonlinear (GRC)	Thermal	√ (Realistic DSTS)	√	√	√	×	×	×
Das, M.K. et al. [31]	2021	PID-RLNN	GOA	Linear	Thermal-hydro-diesel	√ (WT)	×	√	√	√	×	√ (SMES)
Das, S. et al. [32]	2021	TIDN-(1 + PI)	MBA	Linear	Thermal-hydro	√ (WT, GTPP and wave energy)	×	√	×	×	×	×
Raj, U. et al. [33]	2020	Cascade 2DOF-PIDN-FOID	OISA	Linear	Thermal-hydro-gas-diesel	√ (WT and PV)	√	×	√	×	×	×
Present study		**Optimal MPC**	**STOA**	**Nonlinear (GRC-GDB)**	**Thermal-hydro-diesel**	**√ (WT, PV and STPP)**	√	√	√	√	√	**√ (SMES)**

1 = Unilateral-based transaction, 2 = bilateral transaction, 3 = contract violation transaction, 4 = random load disturbance, and 5 = actual solar radiation.

2. Mathematical Model of Deregulated LFC

The proposed system considered in this paper includes three interconnected plants; the first area comprises reheat thermal, wind power units, and *DISCOs* ($DISCO_1$ and $DISCO_2$). Area 2 includes hydro, diesel power units, and *DISCOs* ($DISCO_3$ and $DISCO_4$). Area 3 consists of reheat thermal, PV with MPPT, and *DISCOs* ($DISCO_5$ and $DISCO_6$). Each plant has SMES; Figure 1 shows the proposed multi-interconnected system topology in the deregulated LFC system. The system construction in the Simulink model is presented in Figure 2.

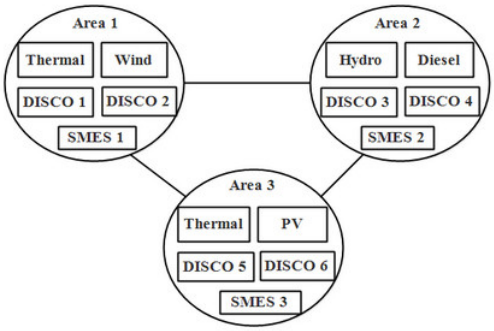

Figure 1. Construction of deregulated multi-interconnected LFC.

In deregulated LFC, contracts conducted via *GENCOs* with *DISCOs* are made based on the *DISCOs* Participation Matrix (*DPM*). The *DISCOs* number represents the column numbers of *DPM*, and the *GENCOs* number is the row numbers of *DPM* in interconnected systems, the sum of each column in the matrix should be equal to unity. The elements of the matrix depend on contract participation factor (*cpf*), and the *DPM* is described by Equation (1).

$$DPM = \begin{bmatrix} cpf_{11} & cpf_{12} & cpf_{13} & cpf_{14} & cpf_{15} & cpf_{16} \\ cpf_{21} & cpf_{22} & cpf_{23} & cpf_{24} & cpf_{25} & cpf_{26} \\ cpf_{31} & cpf_{32} & cpf_{33} & cpf_{34} & cpf_{35} & cpf_{36} \\ cpf_{41} & cpf_{42} & cpf_{43} & cpf_{44} & cpf_{45} & cpf_{46} \\ cpf_{51} & cpf_{52} & cpf_{53} & cpf_{54} & cpf_{55} & cpf_{56} \\ cpf_{61} & cpf_{62} & cpf_{63} & cpf_{64} & cpf_{56} & cpf_{66} \end{bmatrix}, \sum cpf_{ij} = 1 \quad (1)$$

The scheduled steady-state power flow on the tie-line from area i to j is defined as follows:

$dP_{tie,ij\_scheduled}$ = ((demand of *DISCOs* in area$_j$ from *GENCO* in area$_i$) − (demand of *DISCOs* in area$_i$ from *GENCO* in area$_j$))

$$dP_{tie,ij\_scheduled} = \sum_{i=1}^{Dn}\sum_{j=1}^{Gn} dP_{Lj}cpf_{ij} - \sum_{j=1}^{Gn}\sum_{i=1}^{Dn} dP_{Li}cpf_{ij} \quad (2)$$

where Dn is the *DISCOs* number, Gn is the *GENCOs* number, and dP_{Li} is the load disturbance in area i. The actual power flow on tie-line (dP_{tie,ij_actual}) can be described as follows:

$$dP_{tie,ij\_actual} = \left(dF_i - dF_j\right) \times \frac{2\pi T_{ij}}{s} \quad (3)$$

where dF_i and dF_j are the frequency deviations in area i and area j. T_{ij} is the coefficient of synchronizing between areas i and j. The error in tie-line power between area i and area j can be expressed as

$$dP_{tie,ij\_error} = dP_{tie,ij\_actual} - dP_{tie,ij\_scheduled} \quad (4)$$

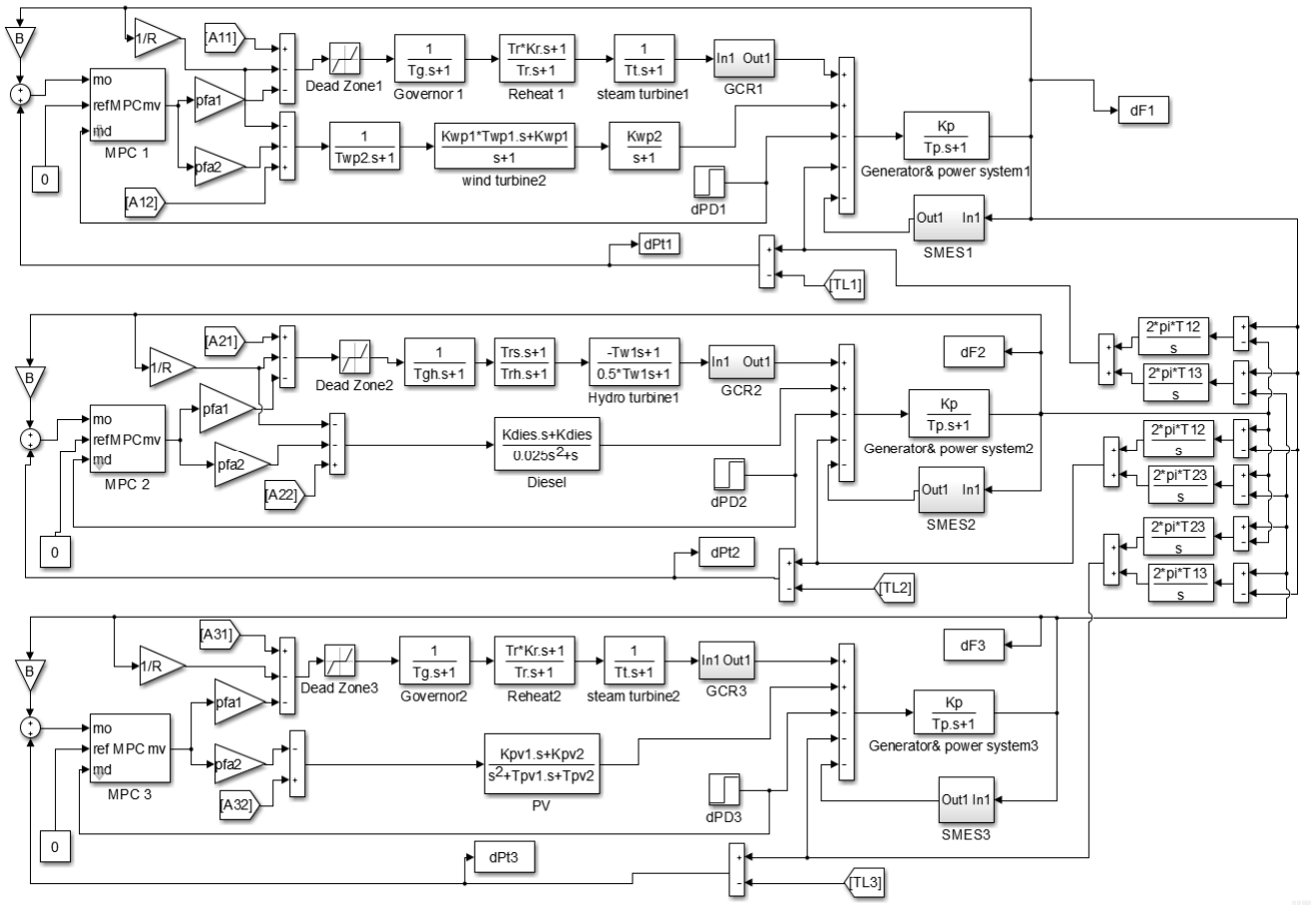

(**a**)

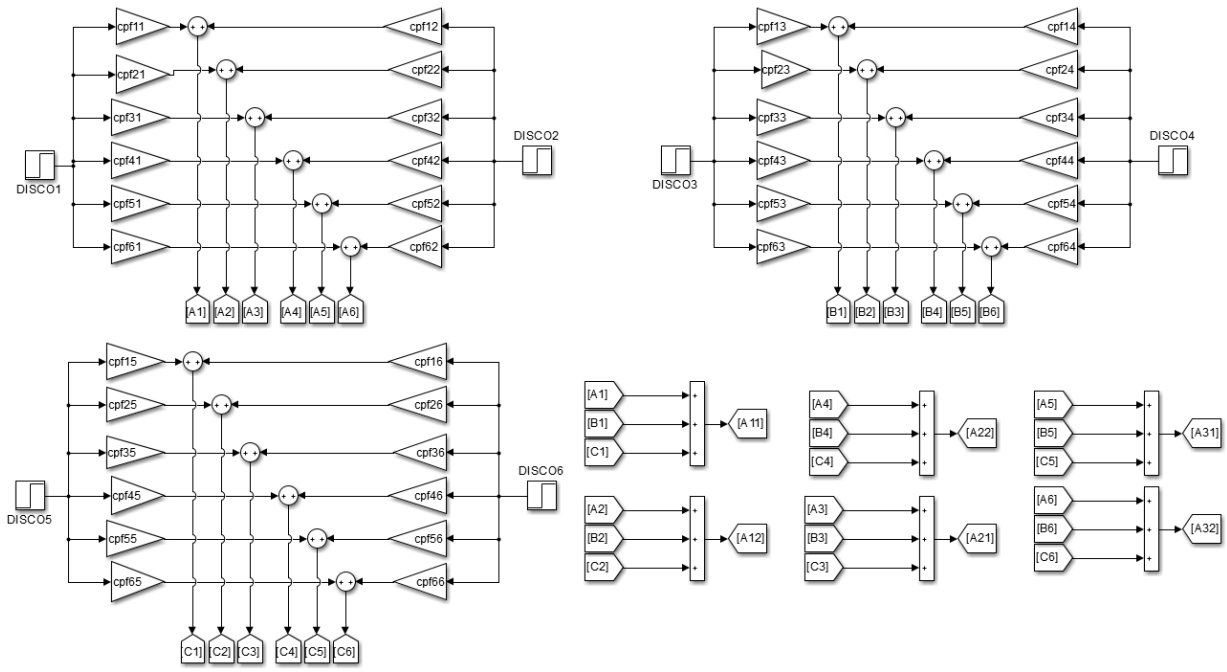

(**b**)

Figure 2. Three interconnected areas with deregulated LFC: (**a**) Simulink model; (**b**) subsystem of the proposed MPC-LFC.

The input signal to MPC is the area control error (*ACE*) which can be written as follows:

$$ACE_i = dF_i \times B_i + dP_{tie,error\_i} \tag{5}$$

where B_i is the bias factor of frequency in area i.

3. Sooty Terns Optimizer Characteristics

Gaurav Dhiman [35] presented the sooty terns optimization algorithm (STOA) in 2019. Sooty terns are wide range of types with variable sizes and weights, they are sea birds that eat amphibians, earthworms, insects, fish, reptiles, etc. Sooty terns (STs) establish the sound of rain, such as catching worms concealed underground by feet and using crumbs of baking to entice the fish. Generally, STs live in colonies and use their cleverness to locate their prey and attack it. Immigration and attacking the prey are prominent aspects of STs behaviors, and migration is identified as the movement of seasonal STs to search for food-rich areas that provide adequate energy. During migration, the STs move in groups following the strongest one and, therefore, they adjust their initial positions to avoid collision with each other. The behavior of STs during migration can be described as follows:

$$\vec{C}_{st} = S_A \times \vec{P}_{st}(z) \tag{6}$$

$$S_A = C_f - z \times \frac{C_f}{Iter_{max}} \tag{7}$$

where $\vec{C}_{st}$ is the position of a sooty tern that does not conflict with another one, $\vec{P}_{st}$ represents the ST's current position, z represents current iteration, S_A is ST motion in a certain search area, while C_f is a variable controlling to set S_A. STs search for the best neighbor and converge with it after avoiding a clash based on the following equation:

$$\vec{M}_{st} = C_B \times (\vec{P}_{bst}(z) - \vec{P}_{st}(z)) \tag{8}$$

$$C_B = 0.5 \times R_{and} \tag{9}$$

where $\vec{M}_{st}$ refers to STs' different positions, $\vec{P}_{bst}$ is the best ST, C_B is a random variable, while R_{and} refers to random number in scale of [0, 1]. The ST or search agent can refresh its location with regards to the best ST.

$$\vec{D}_{st} = \vec{C}_{st} + \vec{M}_{st} \tag{10}$$

where $\vec{D}_{st}$ indicates the disparity between the ST and the fittest ST. When attacking the prey, STs change their speeds and create a spiral behavior which is defined as follows:

$$x' = R_{adi} \times sin(i) \tag{11}$$

$$y' = R_{adi} \times cos(i) \tag{12}$$

$$z' = R_{adi} \times i \tag{13}$$

$$r = u \times e^{kv} \tag{14}$$

where R_{adi} refers to the radius of every spiral turn, i is variable in scale $[0 \leq k \leq 2\pi]$, v and u identify the constant of spiral form, and e refers to normal logarithm. STs update their positions based on the following equation:

$$\vec{P}_{st}(z) = \vec{D}_{st} \times (x' + y' + z') \times \vec{P}_{bst}(z) \tag{15}$$

where $\vec{P}_{st}(z)$ updates the position of another ST and saves the optimal solution.

4. The Proposed Approach

This section presents the major structure of MPC. Additionally, it clarifies the proposed approach combining MPC and STOA.

4.1. Model-Predictive Control (MPC)

MPC is a modern control concept that relies on future predictions to resolve the trouble under study. MPC is commonly utilized in the manufacturing systems. The MPC has many advantages, such as combinations of direct variables, system delay compensation, the ability to handle limitations, and online optimization. Figure 3 presents the MPC structure, which has prediction and controller units [36,37]. The unit of prediction predicts the future results of the system according to its current output, while the control unit utilizes the forecast output to reduce the restrictive equation of the objective function. If restrictions exist, the objective function can be reduced by utilizing the performance prediction function via the control unit. The basic concept of MPC relies on the calculation of the difference between the reference signal and the plant's actual output. The future output is then estimated over time intervals, known as sampling, until the output matches the reference signal.

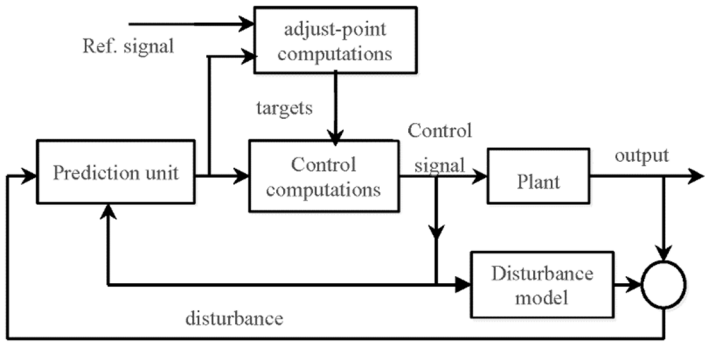

Figure 3. MPC block diagram.

In the MPC algorithm, the system can be described as linear or nonlinear. The plant input and output are presented in the following formula:

$$x(k+1) = Ax(k) + BS_i u_p(k) \tag{16}$$

$$y(k) = {S_o}^{-1} Cx(k) + {S_o}^{-1} DS_i up(k) \tag{17}$$

where A, B, C, and D represent the system state-space matrices, S_o and S_i indicate the output and input diagonal array, respectively, while u_p refers to a nondimensional vector of input variables. The input of MPC can be calculated as $(u(k) = u(k-1) + \Delta u(k))$; by solving the problem with respect to sequence of input, one can get the following expression:

$$min_{\Delta u(k),\ldots,\Delta u(k+M-1)} \left\{ \sum_{j=0}^{M-1} \Delta u^T(k+j) R \Delta u(k+j) + \sum_{i=0}^{P-1} \Delta y^T(k+i) Q \Delta y(k+i) \right\} \tag{18}$$

where M refers to the control horizon, P refers to the prediction horizon $(1 \leq M \leq P)$, T is the sample time, Q and R represent weighting factors, while $y(k+i|k)$ refers to the forecasted output.

4.2. Optimal Deregulated LFC Solving Problem

This section introduces the deregulated LFC using MPC optimized via the proposed STOA. The MPC parameters (M, P, T, Q, and R) are identified via the proposed methodol-

ogy of STOA to minimize the ITAE of aberrations in frequencies and powers in tie-lines as follows:

$$ITAE = \int_0^t \sum_{i=1}^{n} (|dF_i| + |dP_{tie,i}|)\, t.dt \tag{19}$$

where t and n are the time of simulation and area number, dF_i is the frequency deviation in area i, and $dP_{tie,i}$ refers to the deviation in tie-line power of area i. In this work, the MPC design is based on linear time invariant (LTI) which can be determined through MPC toolbox for each area with the aid of Matlab/Simulink. Figure 4 shows the MPC adaptation mechanism implemented through the suggested STOA; the MPC parameters' constraints are selected as $1 \leq M$, $1 \leq P$, $1 \leq R$, $Q \leq 10$, and $0.1 \leq T \leq 10$. The MPC is fed by three inputs which are reference signal, deviation in frequency of the LFC system, and load disturbance measurement. The ITAE is computed depending on current aberrations in frequencies and powers in tie-lines and then fed to the proposed STOA. The MPC optimum parameters can be identified by STOA through minimizing the ITAE. Figure 5 explains the steps for implementing the proposed STOA.

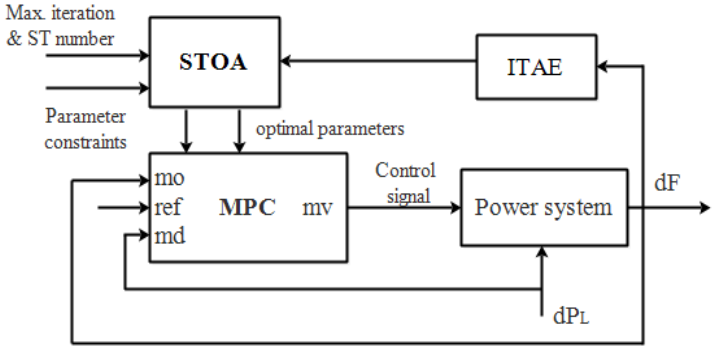

Figure 4. The suggested MPC adjusted by STOA.

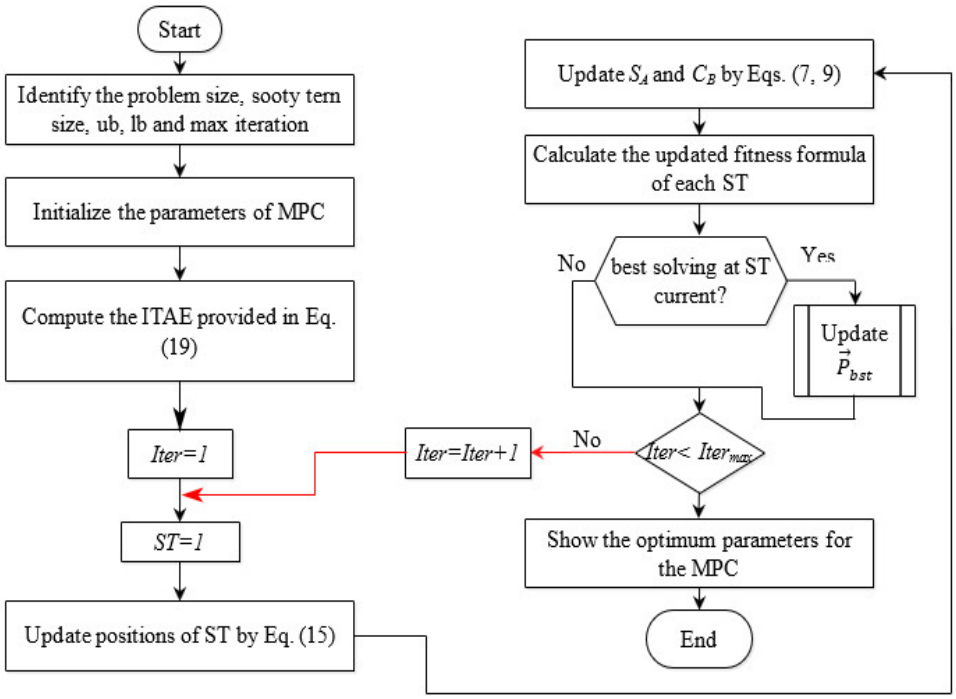

Figure 5. Flowchart of proposed STOA to optimize MPC-LFC.

5. Simulation Results

In this work, the MPC optimal parameters are determined via the proposed STOA-based deregulated LFC installed in multi-interconnected plants with RESs and SMES. The controlling parameters of STOA are assigned as 50 for population size, and maximum iteration of 100. The proposed approach is applied on the system shown in Figure 2 which consists of nonlinear three areas with multi-sources and deregulated LFC environment through three cases. The proposed system parameters are tabulated in Table A1 in Appendix A, while governor dead band (GDB) and generation rate constraint (GRC) are specified to be 3%. The obtained results via the proposed approach are compared to those obtained by MPC optimized via differential evolution (DE), stain bower braid algorithm (SBO), firefly algorithm (FA), and intelligent water drops algorithm (IWD).

5.1. Unilateral-Based Transaction

In this case, there is unilateral contract between *DISCOs* and *GENCOs* in area 1; this can be represented as given in Equations (20) and (21). The demand power is 0.005 pu for $DISCO_1$ and $DISCO_2$ ($DISCO_1 = DISCO_2 = 0.005$), while the total load disturbance in area 1 (dP_{D1}) is 0.01 pu, which presents the sum demand load in $DISCO_1$ and $DISCO_2$. However, there is no demand for power by $DISCO_3$, $DISCO_4$, $DISCO_5$, $DISCO_6$, and load disturbance in areas 2 and 3.

$$DPM = \begin{bmatrix} 0.5 & 0.5 & 0 & 0 & 0 & 0 \\ 0.5 & 0.5 & 0 & 0 & 0 & 0 \\ 0 & 0 & 0 & 0 & 0 & 0 \\ 0 & 0 & 0 & 0 & 0 & 0 \\ 0 & 0 & 0 & 0 & 0 & 0 \\ 0 & 0 & 0 & 0 & 0 & 0 \end{bmatrix} \tag{20}$$

$$\begin{aligned} dPD_1 &= DISCO_1 + DISCO_2 = 0.01\ pu \\ dPD_2 &= DISCO_3 + DISCO_4 = 0\ pu \\ dPD_3 &= DISCO_5 + DISCO_6 = 0\ pu \end{aligned} \tag{21}$$

The change in the response of the generation units for each GENCO can be written as follows:

$$dP_{GENCO_1} = \sum_{j=1}^{6} cpf_{1j} \times dDISCO_j = (0.5 + 0.5) \times 0.005 = 0.005\ pu.MW \tag{22}$$

$$dP_{GENCO_2} = \sum_{j=1}^{6} cpf_{2j} \times dDISCO_j = (0.5 + 0.5) \times 0.005 = 0.005\ pu.MW \tag{23}$$

Table 3 illustrates the errors (integral absolute error (IAE), integral square error (ISE), integral time absolute error (ITAE), and integral time square error (ITSE)) that are obtained by the different algorithms compared to the proposed technique with/without SMES. The optimum parameters of MPC-based deregulated LFC obtained by the presented methodologies are illustrated in Table 4. The aberrations in frequencies and powers flow in tie-lines are shown in Figure 6, while Table 5 presents the system performance specifications including peak undershoot (PUs), peak overshoot (POs), and settling time (Ts) of the fluctuations in frequencies and powers in tie-lines. The settling time and overshoot are minimized by the proposed STOA with/without SMES.

Table 3. Different errors obtained by the suggested STOA compared to different algorithms.

Algorithm	ITAE	IAE	ITSE	ISE
GOA [31]	1.5881	0.1035	0.00064	0.00012
IWD	1.6434	0.1796	0.0022	0.0006
FA	1.5204	0.2097	0.0036	0.00099
DE	0.7078	0.1176	0.00096	0.00041
SBO	0.9502	0.1573	0.0020	0.00073
STOA	0.3736	0.0862	0.00057	0.00036
STOA with SMES	0.1302	0.0357	0.00011	0.00011

Table 4. MPC optimal parameters with unilateral-based transaction obtained via the presented methodologies.

Algorithm	Cont.	Parameter				
		T	P	M	R	Q
IWD	MPC1	1.0188	4.0000	3.6313	8.0187	9.4088
	MPC2	1.4835	7.0000	3.0423	1.2121	4.1062
	MPC3	1.7736	9.0000	2.3223	5.8237	2.5449
FA	MPC1	4.5778	7.0000	2.9508	7.1024	4.9171
	MPC2	7.9330	7.0000	2.8788	6.8717	2.1063
	MPC3	4.1919	7.0000	2.5025	6.3966	6.1616
DE	MPC1	0.1058	10.000	1.0000	9.5576	1.8960
	MPC2	0.1714	10.000	1.0316	1.0000	9.9312
	MPC3	8.0646	4.0000	1.0000	9.7133	7.2729
SBO	MPC1	2.2503	7.0000	3.4737	4.2343	8.6914
	MPC2	7.2548	7.0000	2.0266	7.2507	1.9411
	MPC3	6.6740	8.0000	3.2194	8.8556	9.1734
STOA	MPC1	0.1015	10.000	1.6962	1.0000	4.7993
	MPC2	0.1425	5.0000	1.0000	1.0098	10.000
	MPC3	0.1000	5.0000	2.1788	1.0037	10.000
STOA with SMES	MPC1	0.9897	6.0000	3.0211	1.0000	10.000
	MPC2	0.1114	9.0000	1.0329	1.0000	3.6893
	MPC3	0.1163	7.0000	3.7377	9.3049	1.0792

Table 5. Performance analysis of unilateral-based transaction.

Sig.	MPC via IWD			MPC via FA			MPC via DE		
	Ts (s)	PUs (Hz)	Pos (Hz)	Ts (s)	PUs (Hz)	Pos (Hz)	Ts (s)	PUs (Hz)	Pos (Hz)
dF1	27.0376	−0.0086	0.0168	19.0569	−0.0067	0.0179	14.6580	−0.0066	0.0164
dF2	31.1874	−0.0056	0.0052	31.7522	−0.0004	0.0007	20.7756	−0.0019	0.0066
dF3	33.0361	−0.0048	0.0080	32.3542	−0.0058	0.0090	26.9215	−0.0039	0.0081
dPtie1	25.2028	−0.0048	0.0062	25.3927	−0.0016	0.0102	21.6732	−0.0029	0.0061
dPtie2	28.6876	−0.0049	0.0033	26.9591	−0.0092	0.0018	22.6277	−0.0047	0.0023
dPtie3	49.6124	−0.0032	0.0024	35.4933	−0.0034	0.0021	31.1791	−0.0031	0.0015
	MPC via SBO			**MPC via STOA**			**MPC via STOA with SMES**		
dF1	19.7260	−0.0075	0.0187	10.0692	−0.0064	0.0178	10.9544	−0.0055	0.0133
dF2	29.1531	−0.0004	0.0007	15.7320	−0.0020	0.0053	7.8413	−0.0003	0.0022
dF3	28.6542	−0.0062	0.0093	11.3257	−0.0078	0.0119	10.3924	−0.0006	0.0024
dPtie1	21.2646	−0.0016	0.0083	10.9328	−0.0028	0.0069	10.2124	−0.0012	0.0045
dPtie2	20.5120	−0.0097	0.0010	10.9060	−0.0046	0.0026	9.3023	−0.0024	0.0006
dPtie3	33.0939	−0.0035	0.0022	10.7960	−0.0032	0.0022	10.2997	−0.0021	0.0006

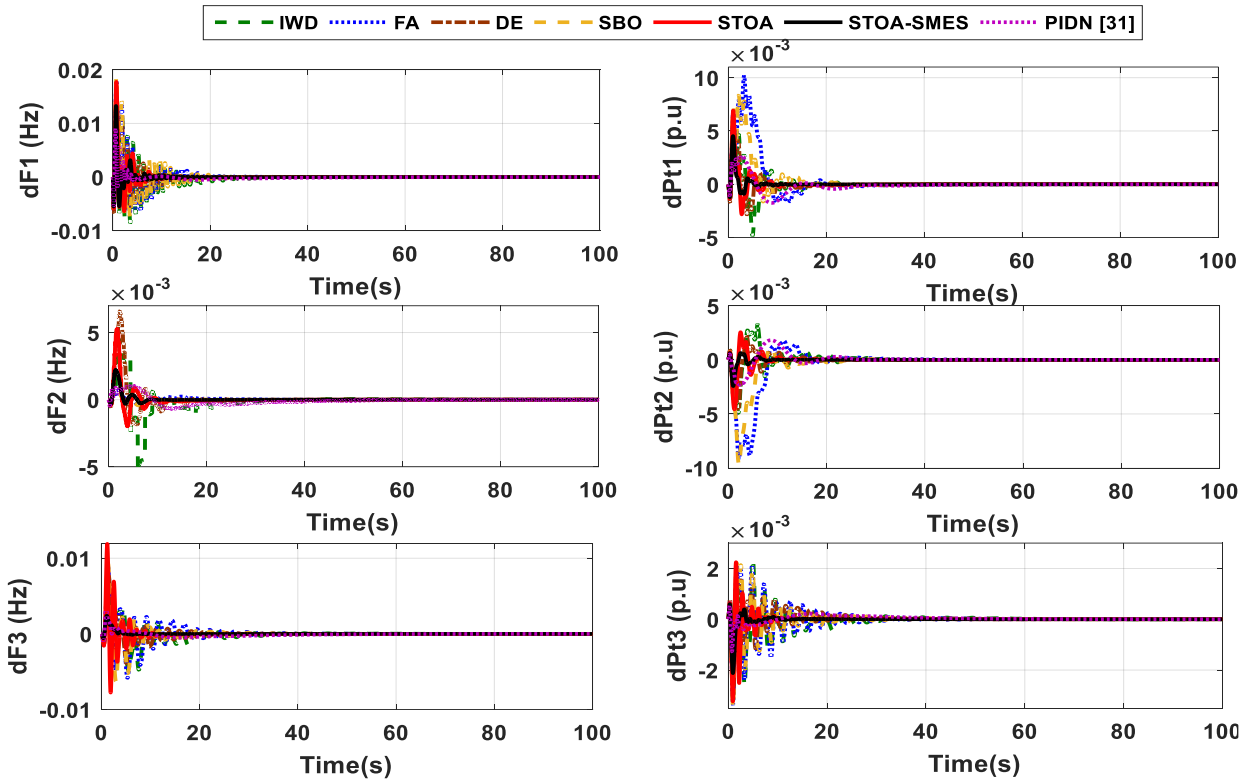

Figure 6. Time response of dF and dP_{tie} for unilateral-based transaction.

5.2. Bilateral Transaction

In this case, the *DISCOs* contract with any *GENCOs* are bound by the terms of the contract concluded between them. Assume that the power demand for each DISCO is 0.005 ($DISCO_1 = DISCO_2 = DISCO_3 = DISCO_4 = DISCO_5 = DISCO_6 = 0.005$), while the total load disturbance in all areas is 0.01 pu ($dP_{D1} = dP_{D2} = dP_{D3} = 0.01$ pu), and the *DPM* is assigned as in Equation (24).

$$DPM = \begin{bmatrix} 0.3 & 0.25 & 0.3 & 0.2 & 0.2 & 0 \\ 0.2 & 0.15 & 0 & 0.2 & 0.1 & 0 \\ 0 & 0.15 & 0.4 & 0 & 0.2 & 0.4 \\ 0.2 & 0.15 & 0 & 0.2 & 0.2 & 0.1 \\ 0.2 & 0.15 & 0.3 & 0.3 & 0.2 & 0.5 \\ 0.1 & 0.15 & 0 & 0.1 & 0.1 & 0 \end{bmatrix} \quad (24)$$

$$\begin{aligned} dPD_1 &= DISCO_1 + DISCO_2 = 0.01\ pu \\ dPD_2 &= DISCO_3 + DISCO_4 = 0.01\ pu \\ dPD_3 &= DISCO_5 + DISCO_6 = 0.01\ pu \end{aligned} \quad (25)$$

The power change of the generation units for each *GENCO* is illustrated as follows:

$$dP_{GENCO_1} = \sum_{j=1}^{6} cpf_{1j} \times dDISCO_j = (0.3 + 0.25 + 0.3 + 0.2 + 0.2 + 0) \times 0.005 = 0.00625\ pu.MW \quad (26)$$

$$dP_{GENCO_2} = \sum_{j=1}^{6} cpf_{2j} \times dDISCO_j = (0.2 + 0.15 + 0 + 0.2 + 0.1 + 0) \times 0.005 = 0.00325\ pu.MW \quad (27)$$

$$dP_{GENCO_3} = \sum_{j=1}^{6} cpf_{3j} \times dDISCO_j = (0 + 0.15 + 0.4 + 0 + 0.2 + 0.4) \times 0.005 = 0.00575\ pu.MW \quad (28)$$

$$dP_{GENCO_4} = \sum_{j=1}^{6} cpf_{4j} \times dDISCO_j = (0.2 + 0.15 + 0 + 0.2 + 0.2 + 0.1) \times 0.005 = 0.00425\ pu.MW \quad (29)$$

$$dP_{GENCO_5} = \sum_{j=1}^{6} cpf_{5j} \times dDISCO_j = (0.2 + 0.15 + 0.3 + 0.3 + 0.2 + 0.5) \times 0.005 = 0.00825\ pu.MW \quad (30)$$

$$dP_{GENCO6} = \sum_{j=1}^{6} cpf_{6j} \times dDISCO_j = (0.1 + 0.15 + 0 + 0.1 + 0.1 + 0) \times 0.005 = 0.00225\ pu.MW \quad (31)$$

The best obtained fitness function is via the proposed approach compared to IWD, FA, DE, and SBO, as tabulated in Table 6. MPC optimum parameters obtained by different approaches with deregulated LFC under bilateral transaction case are tabulated in Table 7. Aberrations in frequencies and powers in tie-lines are shown in Figure 7. Table 7 introduces the system performance specifications for curves presented in Figure 7. The effect of installed SMES in the system to minimize ITAE is clarified and given in Table 6, Table 8 and Figure 7.

Table 6. The errors given by the suggested STOA compared to different algorithms.

Algorithm	ITAE	IAE	ITSE	ISE
IWD	35.6750	2.1620	0.2921	0.0385
FA	33.2202	2.4408	0.4506	0.0499
DE	30.1369	2.3571	0.4204	0.0493
SBO	32.1007	2.3821	0.4301	0.0487
STOA	3.2369	0.3996	0.0102	0.0028
STOA with SMES	0.6619	0.1343	0.0011	0.00055

Table 7. MPC optimal parameters with deregulated LFC obtained by different approaches.

Algorithm	Cont.	Parameter				
		T	P	M	R	Q
IWD	MPC1	6.1667	8.0000	3.7863	8.2602	6.2492
	MPC2	2.0503	5.0000	3.8281	1.4377	5.5301
	MPC3	1.8900	10.000	3.5589	5.8544	5.7842
FA	MPC1	6.8705	6.0000	2.5811	6.4681	3.3892
	MPC2	2.3363	7.0000	2.5216	5.2274	5.8524
	MPC3	9.3026	8.0000	1.6665	7.1737	4.7571
DE	MPC1	2.5035	4.0000	2.2353	7.0311	1.8310
	MPC2	2.6587	6.0000	3.6384	2.6987	9.4498
	MPC3	9.4381	4.0000	1.6674	10.000	6.0715
SBO	MPC1	2.9720	7.0000	1.2831	9.6783	2.6398
	MPC2	1.1842	6.0000	1.6785	4.3008	4.5068
	MPC3	9.3530	10.000	1.1492	6.9536	5.1313
STOA	MPC1	0.3460	10.000	3.1737	1.0000	1.1277
	MPC2	5.4724	6.0000	3.3661	1.0000	7.1087
	MPC3	0.1000	4.2887	4.0000	1.0000	10.000
STOA with SMES	MPC1	0.1068	4.0000	3.1802	1.2149	7.1680
	MPC2	0.1051	4.0000	1.8494	1.1014	7.6772
	MPC3	0.1000	5.0000	3.2439	1.0000	10.000

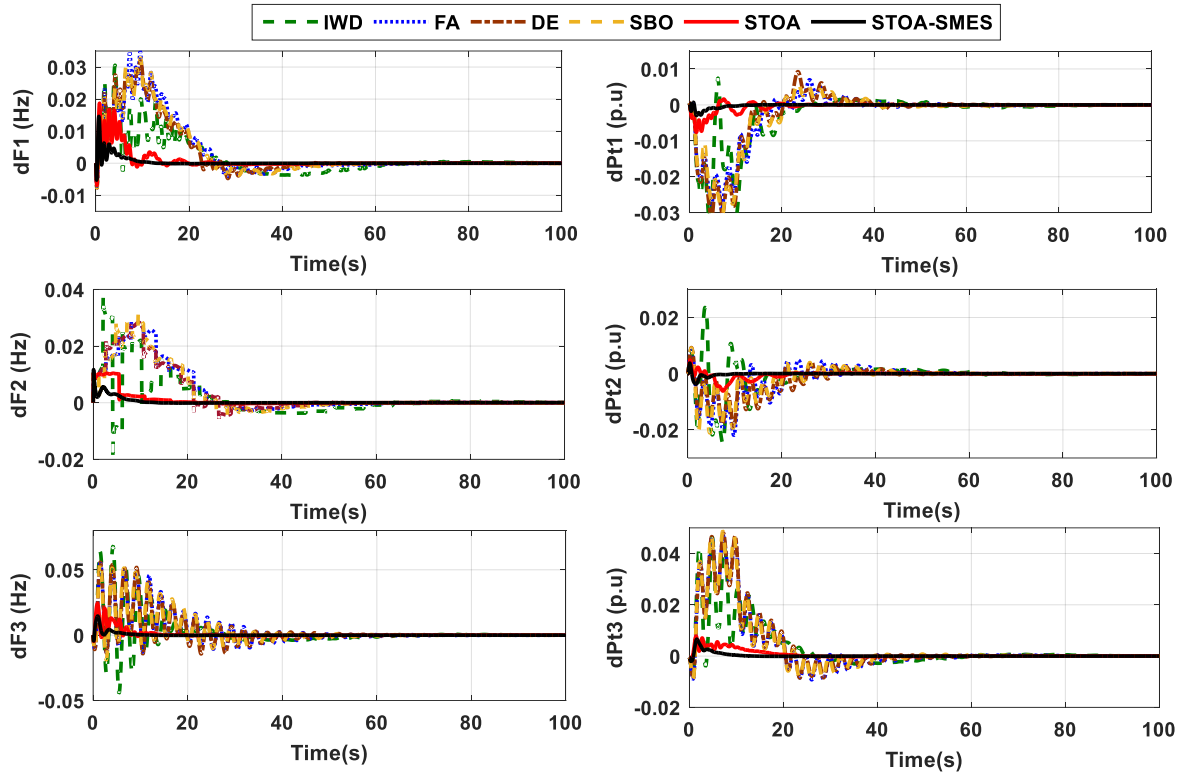

Figure 7. Aberrations in dF and dP_{tie} under bilateral transaction case.

Table 8. Performance analysis bilateral transaction.

Sig.	MPC via IWD			MPC via FA			MPC via DE		
	Ts (s)	PUs (Hz)	Pos (Hz)	Ts (s)	PUs (Hz)	Pos (Hz)	Ts (s)	PUs (Hz)	Pos (Hz)
dF1	63.9004	−0.0072	0.0306	53.6476	−0.0074	0.0349	43.7017	−0.0078	0.0319
dF2	63.5724	−0.0199	0.0376	53.3038	0.0026	0.028	45.2208	−0.0057	0.0284
dF3	60.1116	−0.0442	0.0680	56.1535	−0.0142	0.0566	52.0592	−0.0143	0.0558
dPtie1	68.2425	−0.0306	0.0075	45.1001	−0.0292	0.0070	42.9730	−0.0317	0.0092
dPtie2	61.5340	−0.0246	0.0236	54.0869	−0.0219	0.0048	51.4809	−0.0189	0.0042
dPtie3	54.8649	−0.0039	0.0463	49.0363	−0.0092	0.0469	46.4990	−0.0085	0.0480
	MPC via SBO			**MPC via STOA**			**MPC via STOA with SMES**		
dF1	50.5606	−0.0077	0.0328	21.8899	−0.0069	0.0187	11.4348	−0.0053	0.0146
dF2	49.7371	−0.0046	0.0315	41.6452	−0.0004	0.0105	10.6745	−0.0001	0.0117
dF3	55.3097	−0.0188	0.0553	18.4991	−0.0048	0.0242	9.9298	−0.0044	0.0146
dPtie1	42.3331	−0.0306	0.0061	24.2308	−0.0076	0.0016	14.1611	−0.0030	0.0007
dPtie2	51.1851	−0.0211	0.0044	46.4254	−0.0062	0.0023	9.5737	−0.0037	7.3×10^{-5}
dPtie3	45.8561	−0.0089	0.0487	41.7109	−0.0002	0.0078	11.7334	-9.9×10^{-5}	0.0066

5.3. Contract Violation Transaction

Usually, the demand for power increases and *DISCOs* strive to achieve the profits, therefore there is a violation of contracts with the *GENCOs*. The *GENCOs* must meet the increase of power demand from *DISCOs*. Given the contracting procedures mentioned in Section 5.2 and Equations (22) and (23), the power demand requested by the $DISCO_1$ and $DISCO_2$ are modified to 0.01, while the other *DISCOs* requests remain the same, at 0.005.

Moreover, the power change of the $GENCO_1$, $GENCO_2$, and load disturbance in all areas are given as follows:

$$\begin{array}{l} dPD_1 = DISCO_1 + DISCO_2 = 0.02\ pu \\ dPD_2 = DISCO_3 + DISCO_4 = 0.01\ pu \\ dPD_3 = DISCO_5 + DISCO_6 = 0.01\ pu \end{array} \quad (32)$$

$$dP_{GENCO_1} = \sum_{j=1}^{6} cpf_{1j} \times dDISCO_j = (0.3 + 0.25 + 0.3 + 0.2 + 0.2 + 0) \times 0.01 = 0.0125\ pu.MW \quad (33)$$

$$dP_{GENCO_2} = \sum_{j=1}^{6} cpf_{2j} \times dDISCO_j = (0.2 + 0.15 + 0 + 0.2 + 0.1 + 0) \times 0.01 = 0.0065\ pu.MW \quad (34)$$

When the system given in Figure 2 is simulated under this case, the ITAE obtained via the proposed STOA is 1.0102. Table 9 presents a comparison between the values of errors obtained by the proposed approach and the other simulated algorithms. The MPC optimum parameters obtained by different approaches with deregulated LFC are presented in Table 10. The frequencies and tie-line powers' aberrations are displayed in Figure 8. The corresponding performance specifications for such cases are tabulated in Table 11. The settling time and overshoot are minimized by the proposed STOA.

Table 9. The errors obtained via the presented algorithms.

Algorithm	ITAE	IAE	ITSE	ISE
IWD	53.9881	3.1885	0.6218	0.0785
FA	49.0131	3.7460	1.1571	0.1293
DE	46.3893	3.6482	1.0186	0.1222
SBO	47.0683	3.5857	1.0208	0.1184
STOA	5.1892	0.6027	0.0210	0.0056
STOA with SMES	1.0106	0.2071	0.0025	0.0012

Table 10. Optimum parameters of MPC-deregulated LFC under contract violation.

Algorithm	Cont.	Parameter				
		T	P	M	R	Q
IWD	MPC1	6.1667	8.0000	3.7863	8.2602	6.2492
	MPC2	2.0503	5.0000	3.8281	1.4377	5.5301
	MPC3	1.8900	10.000	3.5589	5.8544	5.7842
FA	MPC1	5.2872	6.0000	2.9868	6.3122	4.0850
	MPC2	1.2944	8.0000	1.7920	5.3635	6.3384
	MPC3	9.3368	9.0000	1.5967	4.5315	3.9342
DE	MPC1	10.000	6.0000	1.0000	10.000	4.1331
	MPC2	2.3147	9.0000	2.3905	1.0000	3.4827
	MPC3	9.2692	10.000	1.3768	7.5380	8.5526
SBO	MPC1	2.8428	7.0000	1.0952	9.8400	2.6615
	MPC2	1.3013	6.0000	1.6362	3.7066	5.3726
	MPC3	9.3763	10.000	1.3055	7.5704	3.4958
STOA	MPC1	0.3863	6.0000	1.3697	1.0000	10.000
	MPC2	1.3889	10.000	1.7762	1.0000	10.000
	MPC3	0.1000	4.0000	4.0000	1.0000	10.000
STOA with SMES	MPC1	0.1061	8.0000	1.1080	1.1258	8.9523
	MPC2	0.1092	4.0000	1.2645	2.1158	8.0565
	MPC3	0.1000	7.0000	2.4561	1.0000	10.000

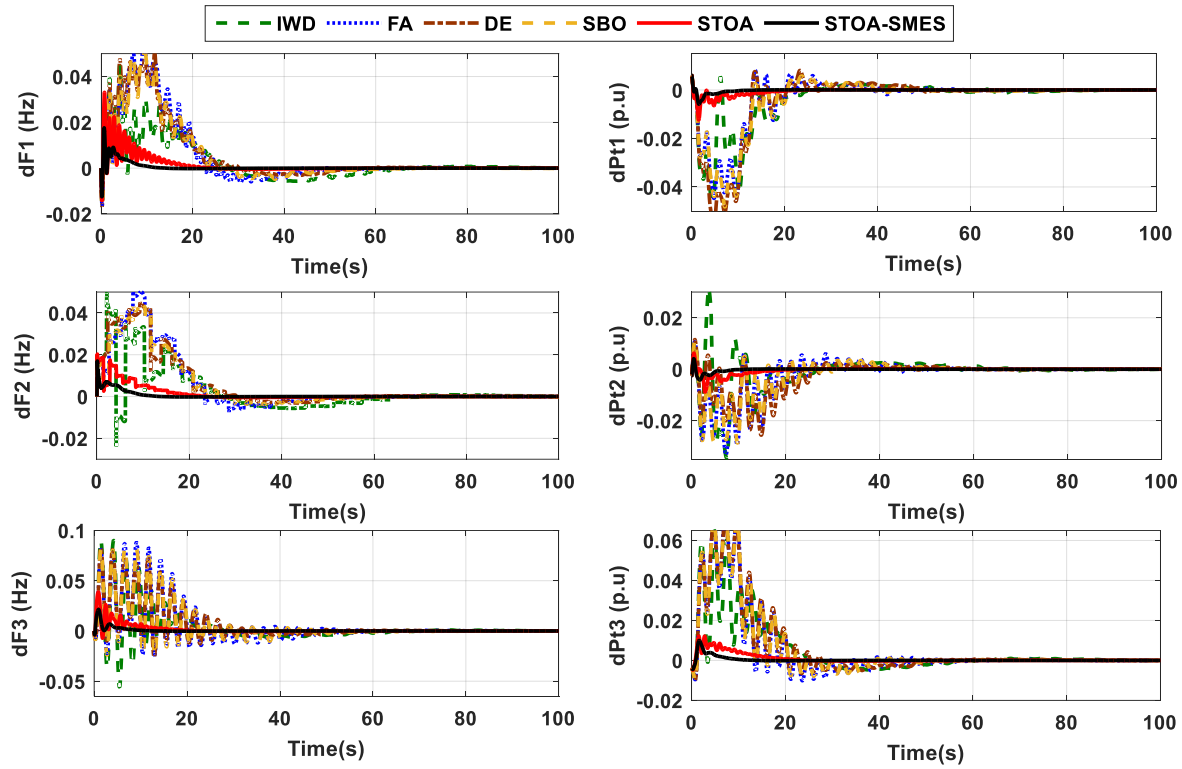

Figure 8. Aberrations in dFi and dP_{tie} under contract violation case.

Table 11. Performance specifications of contract violation transaction.

Sig.	MPC via IWD			MPC via FA			MPC via DE		
	Ts (s)	PUs (Hz)	Pos (Hz)	Ts (s)	PUs (Hz)	Pos (Hz)	Ts (s)	PUs (Hz)	Pos (Hz)
dF1	63.9340	−0.0165	0.0454	47.9268	−0.0166	0.0557	51.4054	−0.0167	0.0507
dF2	63.5803	−0.0238	0.0497	49.1896	−0.0074	0.0511	53.2465	−0.0033	0.0450
dF3	60.3591	−0.0558	0.0901	55.4846	−0.0242	0.0882	53.9884	−0.0259	0.0826
dPtie1	68.2835	−0.0448	0.0054	47.3875	−0.0447	0.0081	47.4371	−0.0558	0.0080
dPtie2	61.5780	−0.0344	0.0305	53.6804	−0.0333	0.0107	54.8810	−0.0256	0.0115
dPtie3	55.0195	−0.0047	0.0649	48.6736	−0.0102	0.0747	49.5926	−0.0066	0.0706
	MPC via SBO			**MPC via STOA**			**MPC via STOA with SMES**		
dF1	53.5217	−0.0168	0.0516	20.5473	−0.0142	0.0331	11.4963	−0.0125	0.0176
dF2	56.2937	−0.0047	0.0450	37.5205	−0.0004	0.0203	11.8392	−0.0002	0.0170
dF3	53.2066	−0.0240	0.0817	19.9847	−0.0073	0.0388	10.6878	−0.0040	0.0214
dPtie1	42.3381	−0.0482	0.0058	22.3325	−0.0124	0.0003	12.8129	−0.0059	0.0005
dPtie2	53.7500	−0.0287	0.0120	35.5661	−0.0088	0.0063	21.0063	−0.0042	0.0041
dPtie3	46.4073	−0.0083	0.0751	41.1126	−0.0003	0.0122	11.7787	−0.0002	0.0099

5.4. Sensitivity Analysis

To confirm the robustness and reliability of the proposed approach-based deregulated LFC, the constructed MPC is investigated under changing of the system parameters and random load disturbance. Sensitivity analysis is conducted on deregulated three interconnected plants with LFC and SMES in bilateral and contract violation transactions cases through changing the system parameters, such as T_g, K_r, T_r, T_t, K_p, and T_p, to ±25% and ±50%. The obtained ITAEs in this case are given in Table 12. The proposed approach has the robust performance and competence under changing the system parameters.

Table 12. Errors of deregulated LFC with changing parameters.

Parameter	Bilateral Transaction				Contract Violation			
	ITAE (0.6619)				ITAE (1.0106)			
	−50%	−25%	+25%	+50%	−50%	−25%	+25%	+50%
Tg	0.6619	0.6619	0.6619	0.6618	1.0106	1.0106	1.0106	1.0106
Kr	0.6619	0.6619	0.6619	0.6618	1.0106	1.0106	1.0106	1.0106
Tr	0.6619	0.6619	0.6619	0.6618	1.0106	1.0106	1.0106	1.0106
Tt	0.6619	0.6619	0.6619	0.6618	1.0106	1.0106	1.0106	1.0106
Kp	0.7049	0.6651	0.6607	0.6606	1.1089	1.0157	1.0094	1.0090
Tp	0.6826	0.6606	0.6640	0.6678	1.0105	1.0094	1.0137	1.0195

The application of random load disturbance is vital as the load demand is not usually constant on the system all the time. To confirm the reliability of the proposed technique, the random load change shown in Figure 9 is applied through the $DISCO_1$ and $DISCO_2$ for the same control values and conditions in contract violation case described in Section 5.3, while the total load on area 1 is the sum of $DISCO_1$ and $DISCO_2$. Figure 10 illustrates the aberrations in frequencies and powers in tie-lines under random load change. As the reader can see, the time responses of frequencies and tie-line powers' violations pass through four time intervals according to the load disturbance shown in Figure 10. The proposed MPC-LFC designed via STOA succeeded in vanishing the perturbations in frequencies and tie-line powers in all intervals, with less oscillations compared to the others. The overshoot and undershoot are minimized by the proposed STOA with/without SMES compared to DE and SBO.

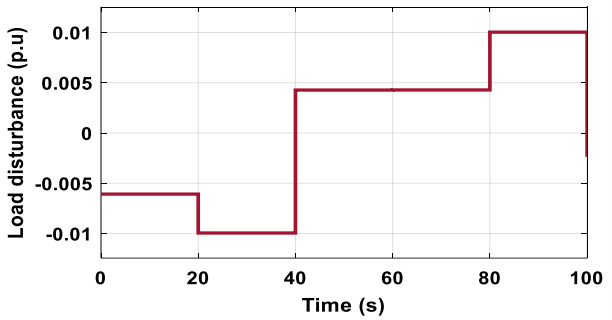

Figure 9. Random load disturbance.

5.5. Practical Case Study

It is important to investigate the proposed MPC-LFC optimized via STOA on a practical plant, this is done by replacing the PV model with the Kuraymat solar thermal power station. Figure 11 shows the location of Kuraymat, which is 90 miles south of Cairo, Egypt. It is a combined cycle plant that has gas turbines with capacity of 80 MW and steam turbine of 40 MW, in addition to one parabolic trough solar system with rating of 20 MW. The solar field covers an area of about 130,800 m^2 and consists of 40 rows of collectors, with each row having four SKAL-ET 150 parabolic trough collectors, and each collector consists of 12 modules [38,39]. In this work, the solar thermal plant is represented in Matlab/Simulink, as shown in Figure 12, to clarify the effect of changing solar radiation on the system. This plant comprises a solar field which represents collectors of parabolic troughs, governor, and steam turbine; the combined heat by collectors is utilized to heat the fluid and water to produce steam and drive the turbine. The recorded solar radiation by the plant shown in Figure 13 is used, and these data are fed to the solar thermal energy unit. The solar radiation was transformed over the day to match the simulation time of the system, and

all conditions and restrictions mentioned in Section 5.2 were applied to obtain the results in this case. The obtained results of the actual case are reported in Table 13, which shows the errors obtained by different approaches at the Kuraymat solar thermal power station. The optimum parameters of MPC obtained by different methodology-based deregulated LFC with solar thermal plant are tabulated in Table 14. The aberrations in frequencies and powers in tie-lines are shown in Figure 14, while Table 15 presents the system performance specifications for curves presented in Figure 14. The settling time and peak overshoot are minimized by the proposed STOA with/without SMES. The obtained results confirm the robustness and competence of the proposed MPC-LFC optimized via STO in this such case.

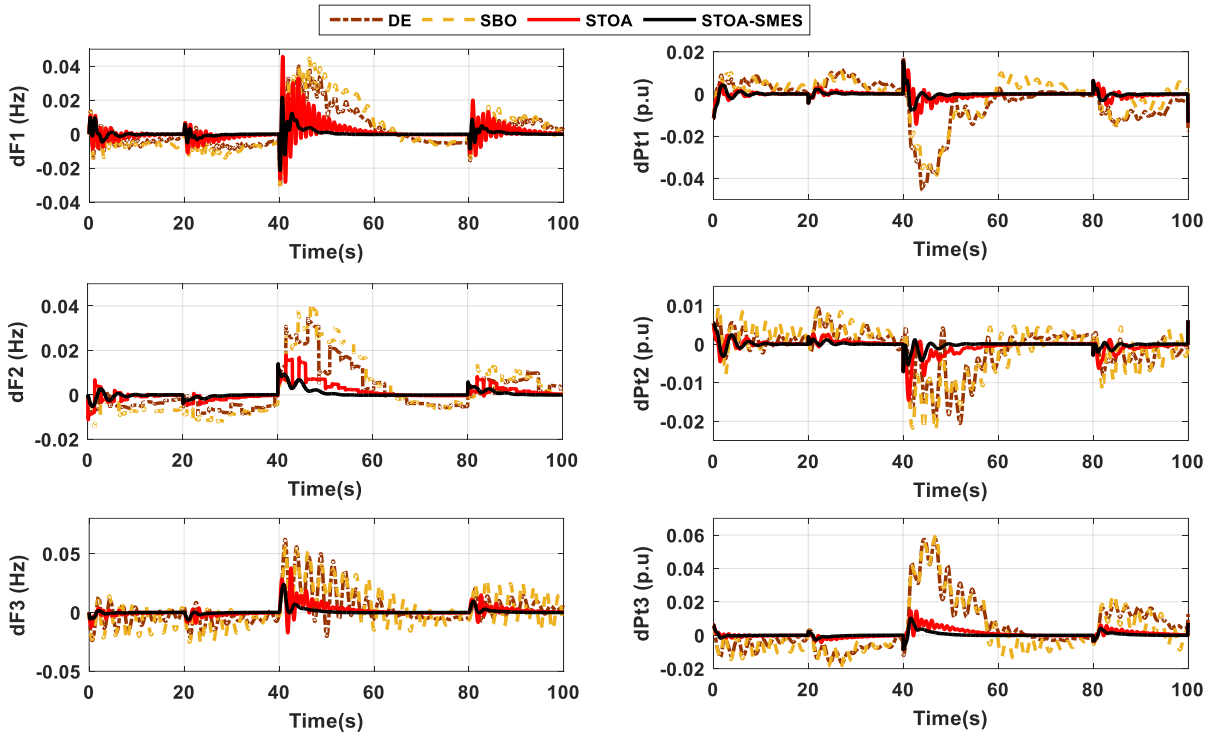

Figure 10. Deviations in dF_i and $dP_{tie,i}$ under random load change.

Figure 11. Location of Kuraymat.

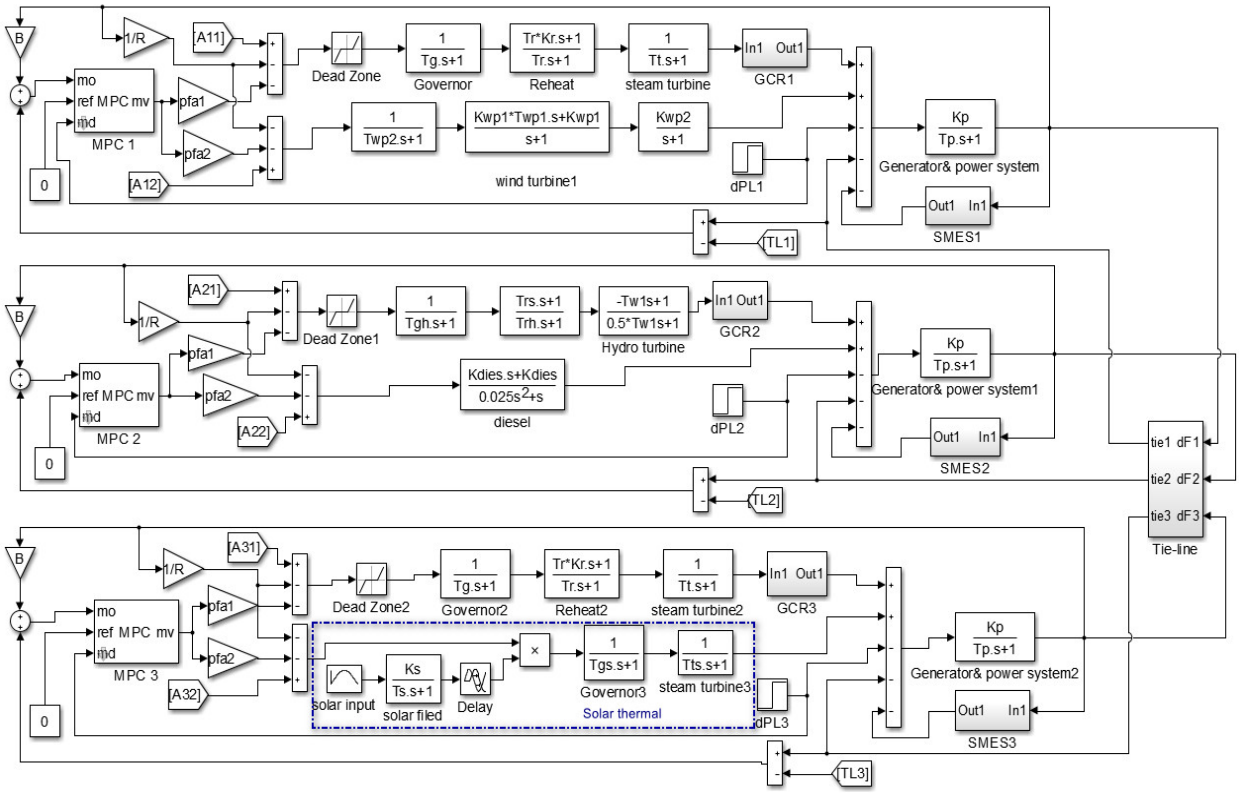

Figure 12. Simulink model of deregulated LFC with solar thermal plant.

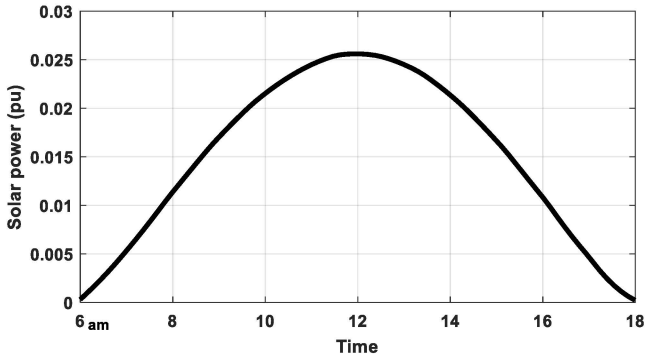

Figure 13. Actual solar radiation of the Kuraymat plant.

Table 13. The errors obtained via the presented algorithms.

Algorithm	ITAE	IAE	ITSE	ISE
IWD	8.1699	0.7598	0.0419	0.0074
FA	5.7623	0.5724	0.0253	0.0052
DE	2.7636	0.2837	0.0054	0.0012
SBO	6.0784	0.5965	0.0230	0.0055
STOA	1.9642	0.2347	0.0036	9.74×10^{-4}
STOA with SMES	0.7647	0.1092	6.65×10^{-4}	3.03×10^{-4}

Table 14. Optimum parameters of MPC-deregulated LFC with solar thermal plant.

Algorithm	Cont.	Parameter				
		T	P	M	R	Q
IWD	MPC1	2.2386	6.0000	2.7958	3.1128	8.6028
	MPC2	2.0960	5.0000	1.7696	3.0907	5.4609
	MPC3	3.2193	10.000	2.8946	2.7096	9.1469
FA	MPC1	2.3419	5.0000	2.5255	3.8603	7.9511
	MPC2	1.1804	5.0000	1.6602	2.6835	5.7731
	MPC3	2.6442	9.0000	2.1220	2.1650	9.2610
DE	MPC1	0.1000	7.0000	2.6028	1.1892	9.7307
	MPC2	0.1003	8.0000	1.0000	1.0010	9.8950
	MPC3	0.1000	10.000	4.0000	1.0007	9.9993
SBO	MPC1	2.2841	6.0000	2.5856	3.1844	8.4974
	MPC2	1.8531	6.0000	1.6108	3.1598	5.2159
	MPC3	3.03711	9.0000	2.3412	1.0113	9.2644
STOA	MPC1	0.1306	6.0000	1.1957	1.6546	4.2269
	MPC2	0.1072	10.000	1.4580	1.2117	4.0086
	MPC3	0.1000	4.0000	1.2055	1.0000	10.0000
STOA with SMES	MPC1	0.1000	5.0000	3.2188	1.0000	10.000
	MPC2	0.1000	10.000	1.9825	1.0000	8.5687
	MPC3	0.1000	5.0000	1.1332	1.0000	10.000

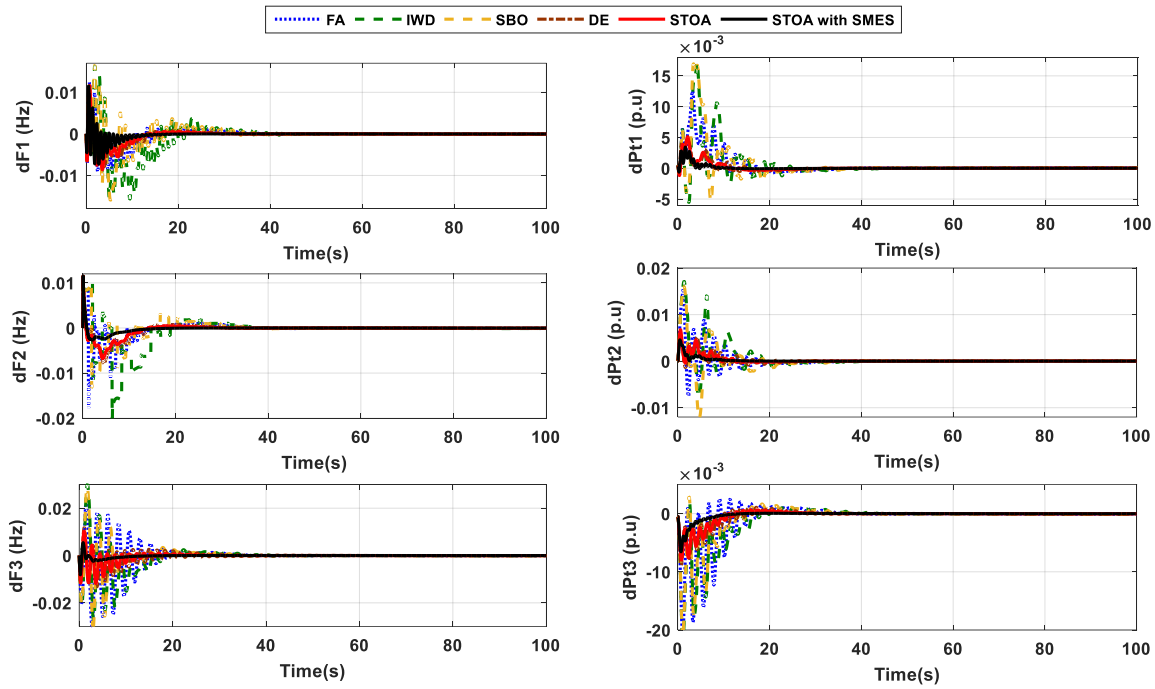

Figure 14. Aberrations in dFi and dP_{tie} under bilateral transaction with solar thermal plant.

Table 15. Performance specifications of the interconnected system with solar thermal plant.

Sig.	MPC via IWD			MPC via FA			MPC via DE		
	Ts (s)	**PUs (Hz)**	**Pos (Hz)**	**Ts (s)**	**PUs (Hz)**	**Pos (Hz)**	**Ts (s)**	**PUs (Hz)**	**Pos (Hz)**
dF1	38.2310	−0.0157	0.0163	35.5070	−0.0091	0.0124	29.0191	−0.0079	0.0098
dF2	33.5896	−0.0207	0.0106	33.0856	−0.0178	0.0106	28.0973	−0.0078	0.0117
dF3	34.2854	−0.0273	0.0300	33.3888	−0.0297	0.0240	38.2454	−0.0132	0.0118
dPtie1	32.4268	−0.0055	0.0172	31.6296	−0.0011	0.0126	30.9189	−0.0007	0.0047
dPtie2	30.0549	−0.0077	0.0141	29.4559	−0.0075	0.0089	30.1285	−0.0014	0.0051
dPtie3	34.7497	−0.0174	0.0020	31.8582	−0.0187	0.0026	30.9790	−0.0017	0.0011
	MPC via SBO			**MPC via STOA**			**MPC via STOA with SMES**		
dF1	35.4207	−0.016	0.0165	25.3660	−0.0087	0.0117	15.3465	−0.0073	0.0115
dF2	35.2094	−0.0132	0.0106	25.7349	−0.0068	0.0115	14.3275	−0.0027	0.0115
dF3	32.4255	−0.0308	0.0287	26.5229	−0.0118	0.0103	14.9977	−0.0082	0.0054
dPtie1	30.6435	−0.0053	0.0170	27.0556	−0.0012	0.0051	20.9348	−0.0006	0.0034
dPtie2	32.5795	−0.0121	0.0073	22.5349	−0.0004	0.0045	13.8070	-1.6×10^{-6}	9.4805
dPtie3	32.9513	−0.0173	0.0029	27.0283	−0.0005	0.0006	11.7035	-4.5×10^{-5}	5.6×10^{-5}

6. Conclusions

This paper proposed a novel structure of load frequency control (LFC) installed in a multi-interconnected system with renewable energy sources and storage systems. The proposed controller is represented by model predictive control (MPC) optimized via recent metaheuristic optimizer of sooty terns optimization algorithm (STOA). The proposed methodology that incorporated STOA was employed to determine the optimal parameters of MPC-LFC. The presented fitness function to be minimized is the integral time absolute error (ITAE), comprising the frequencies and in tie-lines powers' deviations. The constructed MPC-deregulated LFC was combined in an interconnected nonlinear system involving photovoltaic (PV) with maximum power point tracker (MPPT), wind turbine (WT), and superconducting magnetic energy source (SMES). The system was simulated under deregulated cases as unilateral, bilateral, and contract violation-based transactions with/without SMES. The performance specifications (undershoots, peak overshoot, and settling time) of the time responses for frequencies and tie-line powers' aberrations obtained by the proposed STOA were compared to those of different optimizers in all cases. Moreover, the constructed MPC was examined under changing of the system parameters and random load change. Furthermore, a practical case study interconnecting Kuraymat solar thermal power station with others was analyzed based on actual recorded solar radiation. The best fitness function in unilateral transactions case was 0.3736, obtained via STOA, and 0.1302, when SMES was used. In the bilateral transactions case, the best fitness function was 3.2369, obtained using STOA, and 0.6619, with STOA-SMES. On the other hand, the values of ITAE at the contract violation-based transactions case were 5.1892 and 1.0106 by STOA with/without SMES, respectively. The proposed control achieved minimum target of 1.9642 and 0.7647 by STOA with/without SMES for LFC with solar thermal plant. The obtained results confirm the robustness and reliability of the proposed approach incorporating STOA in minimizing the aberration in frequencies and powers in tie-lines and achieving the system stability during load disturbances in the least time. In future work, enhancement of the STOA algorithm to reduce the consumption time is mandatory.

Author Contributions: Conceptualization, H.H.A. and A.F.; methodology, A.M.A.-S. and A.M.K.; software, H.H.A. and A.F.; validation, H.H.A., H.M.H.F., and A.A.A.-S.; formal analysis, H.H.A., A.F., and H.A.G.; investigation, H.H.A. and H.G; data curation, H.H.A., A.F., and H.M.H.F.; writing—original draft preparation, H.H.A. and A.F.; writing—review and editing, H.M.H.F., A.A.A.-S., and H.A.G.; supervision, A.M.K., A.M.A.-S., and H.A.G. All authors have read and agreed to the published version of the manuscript.

Funding: This research received no external funding.

Acknowledgments: Researchers Supporting Project number (RSP-2021/337), King Saud University, Riyadh, Saudi Arabia.

Conflicts of Interest: The authors declare no conflict of interest.

Nomenclature

STOA	Sooty terns optimization algorithm
ST	Sooty terns
LFC	Load frequency control
SBO	Stain bower braid algorithm
MPC	Model predictive control
FA	Firefly algorithm
TRANSCOs	Transmission companies
DE	Differential evolution
DISCOs	Distribution companies
PUs	Peak undershoot
GENCOs	Generation companies
POs	Peak overshoot
SMES	Superconducting magnetic energy storage
Ts	Settling time
DPM	*DISCOs* Participation Matrix
cpf	contract participation factor
Symbols	
A, B, C and D	The system state space matrices
e	Normal logarithm
dP_{Li}	The load disturbance in area i
R_{adi}	The radius of every spiral turn
T_{ij}	The coefficient of synchronizing between areas i and j
R_{and}	The random number in scale of [0, 1]
C_B	The random variable
dP_{Di}	total load disturbance in area i
$\overrightarrow{\boldsymbol{C}}_{\boldsymbol{st}}$	The position of ST that does not conflict with ST another
$x(k)$	The system state
C_f	Controlling variable
$y(k)$	The system outputs
$\overrightarrow{\boldsymbol{P}}_{\boldsymbol{st}}$	The current position of sooty tern
z	The current iteration
$\overrightarrow{\boldsymbol{P}}_{\boldsymbol{st}}\ (\boldsymbol{z})$	The ST positions of other
u and v	The constant of spiral form
$\overrightarrow{\boldsymbol{D}}_{\boldsymbol{st}}$	The disparity between the ST and excellent fittest ST
K_{dies}	The constant gain of diesel unit
S_o and S_i	the output and input diagonal array
K_g	The gain of steam plant governor
T	Sample time of MPC
K_{gh}	The gain of hydro plant governor
M and P	The control and prediction horizons
K_p	The gain of generator and power system
Q and R	Weighting factors
K_{PV1} and K_{PV2}	The gains of PV system
t	Simulation time
K_{pw1}, K_{pw2} and K_{pw3}	Wind plant gains
dF_i	The frequency deviation of i area
K_r	The gain of reheater

$dP_{tie,i}$	The power deviation of tie-line in area i
K_t	The gain of steam turbine
T_g	Time constant of governor (sec.)
T_r	Time constant of reheater (sec.)
T_{gh}	Time constant of hydro governor (sec.)
T_{rh}	Reset time constants of hydro governor (sec.)
T_p	Time constant of generator and power system (sec.)
T_{rs}	Hydro governor transient droop
T_{PV1} and T_{PV2}	Time constants of PV system (sec.)
T_t	Time constant of steam turbine (sec.)
T_{pw1}, T_{pw2} and T_{pw3}	Time constants of wind plant (sec.)
T_w	Nominal start time of the water in penstock (sec.)

Appendix A

Table A1. Parameters of the deregulated LFC.

Parameter	Value	Parameter	Value	Parameter	Value
T_g	0.08 s	K_{pv1}	−18	K_{diesel}	16.5
T_r	10 s	T_{pv1}	100 s	R	0.425 pu MW/Hz
K_r	0.33 Hz/pu MW	K_{pv2}	900	B	2.4 Hz/pu MW
T_t	0.3 s	T_{pv2}	50 s	apf_1	0.65
K_p	120 Hz/pu MW	K_{wp1}	1.25	apf_2	0.35
T_p	20 s	K_{wp2}	1.4	T_{wp1}	6 s
T_{W1}	1 s	T_{wp2}	0.041 s	T_{rs}	0.513 s
T_{rh}	10 s	T_{gh}	48.7 s	K_s	1.8
T_s	1.8	T_{gs}	1.0	T_{ts}	3.0

	K_{smes}	T_1	T_2	T_3	T_4	T_{smes}
SMES1	0.8550	0.1279	0.1057	0.1000	0.6131	0.0144
SMES2	0.8181	0.1377	0.5205	0.1030	0.4241	0.0849
SMES3	0.5336	0.6088	0.1169	0.3597	0.2014	0.4638

References

1. Veerasamy, V.; Member, S.; Izzri, N.; Wahab, A. A Hankel matrix based reduced order model for stability analysis of hybrid power system using PSO-GSA optimized cascade PI-PD controller for automatic load frequency control. *IEEE Access* **2020**, *8*, 71422–71446. [CrossRef]
2. Arya, Y. AGC of restructured multi-area multi-source hydrothermal power systems incorporating energy storage units via optimal fractional-order fuzzy PID controller. *Neural Comput. Appl.* **2019**, *31*, 851–872. [CrossRef]
3. Panwar, A.; Sharma, G.; Nasiruddin, I.; Bansal, R.C. Frequency stabilization of hydro–hydro power system using hybrid bacteria foraging PSO with UPFC and HAE. *Electr. Power Syst. Res.* **2018**, *161*, 74–85. [CrossRef]
4. Pappachen, A.; Peer Fathima, A. Critical research areas on load frequency control issues in a deregulated power system: A state-of-the-art-of-review. *Renew. Sustain. Energy Rev.* **2017**, *72*, 163–177. [CrossRef]
5. Haes Alhelou, H.; Hamedani-Golshan, M.E.; Zamani, R.; Heydarian-Forushani, E.; Siano, P. Challenges and opportunities of load frequency control in conventional, modern and future smart power systems: A comprehensive review. *Energies* **2018**, *11*, 2497. [CrossRef]
6. Fathy, A.; Kassem, A.M.; Abdelaziz, A.Y. Optimal design of fuzzy PID controller for deregulated LFC of multi-area power system via mine blast algorithm. *Neural Comput. Appl.* **2020**, *32*, 4531–4551. [CrossRef]
7. Tasnin, W.; Saikia, L.C. Impact of renewables and FACT device on deregulated thermal system having sine cosine algorithm optimised fractional order cascade controller. *IET Renew. Power Gener.* **2019**, *13*, 1420–1430. [CrossRef]
8. Pappachen, A.; Peer Fathima, A. Load frequency control in deregulated power system integrated with SMES-TCPS combination using ANFIS controller. *Int. J. Electr. Power Energy Syst.* **2016**, *82*, 519–534. [CrossRef]
9. Morsali, J.; Zare, K.; Tarafdar Hagh, M. A novel dynamic model and control approach for SSSC to contribute effectively in AGC of a deregulated power system. *Int. J. Electr. Power Energy Syst.* **2018**, *95*, 239–253. [CrossRef]

10. Tasnin, W.; Saikia, L.C.; Raju, M. Deregulated AGC of multi-area system incorporating dish-Stirling solar thermal and geothermal power plants using fractional order cascade controller. *Int. J. Electr. Power Energy Syst.* **2018**, *101*, 60–74. [CrossRef]
11. Khamari, D.; Sahu, R.K.; Gorripotu, T.S.; Panda, S. Automatic generation control of power system in deregulated environment using hybrid TLBO and pattern search technique. *Ain Shams Eng. J.* **2020**, *11*, 553–573. [CrossRef]
12. Arya, Y.; Kumar, N. Design and analysis of BFOA-optimized fuzzy PI/PID controller for AGC of multi-area traditional/restructured electrical power systems. *Soft Comput.* **2017**, *21*, 6435–6452. [CrossRef]
13. Mohanty, B. Hybrid flower pollination and pattern search algorithm optimized sliding mode controller for deregulated AGC system. *J. Ambient Intell. Humaniz. Comput.* **2020**, *11*, 763–776. [CrossRef]
14. Kumari, S.; Shankar, G. Maiden application of cascade tilt-integral-derivative controller in load frequency control of deregulated power system. *Int. Trans. Electr. Energy Syst.* **2020**, *30*, e12257. [CrossRef]
15. Nosratabadi, S.M.; Bornapour, M.; Gharaei, M.A. Grasshopper optimization algorithm for optimal load frequency control considering Predictive Functional Modified PID controller in restructured multi-resource multi-area power system with Redox Flow Battery units. *Control Eng. Pract.* **2019**, *89*, 204–227. [CrossRef]
16. Prakash, A.; Murali, S.; Shankar, R.; Bhushan, R. HVDC tie-link modeling for restructured AGC using a novel fractional order cascade controller. *Electr. Power Syst. Res.* **2019**, *170*, 244–258. [CrossRef]
17. Shiva, C.K.; Mukherjee, V. A novel quasi-oppositional harmony search algorithm for AGC optimization of three-area multi-unit power system after deregulation. *Eng. Sci. Technol. Int. J.* **2016**, *19*, 395–420. [CrossRef]
18. Nandi, M.; Shiva, C.K.; Mukherjee, V. TCSC based automatic generation control of deregulated power system using quasi-oppositional harmony search algorithm. *Eng. Sci. Technol. Int. J.* **2017**, *20*, 1380–1395. [CrossRef]
19. Shiva, C.K.; Mukherjee, V. Design and analysis of multi-source multi-area deregulated power system for automatic generation control using quasi-oppositional harmony search algorithm. *Int. J. Electr. Power Energy Syst.* **2016**, *80*, 382–395. [CrossRef]
20. Mohanty, B.; Hota, P.K. Comparative performance analysis of fruit fly optimisation algorithm for multi-area multisource automatic generation control under deregulated environment. *IET Gener. Transm. Distrib.* **2015**, *9*, 1845–1855. [CrossRef]
21. Prakash, A.; Kumar, K.; Parida, S.K. PIDF(1+FOD) controller for load frequency control with sssc and ac-dc tie-line in deregulated environment. *IET Gener. Transm. Distrib.* **2020**, *14*, 2751–2762. [CrossRef]
22. Shankar, R.; Kumar, A.; Raj, U.; Chatterjee, K. Fruit fly algorithm-based automatic generation control of multiarea interconnected power system with FACTS and AC/DC links in deregulated power environment. *Int. Trans. Electr. Energy Syst.* **2019**, *29*, e2690. [CrossRef]
23. Dhundhara, S.; Verma, Y.P. Capacitive energy storage with optimized controller for frequency regulation in realistic multisource deregulated power system. *Energy* **2018**, *147*, 1108–1128. [CrossRef]
24. Ghasemi-marzbali, A. Multi-area multi-source automatic generation control in deregulated power system. *Energy* **2020**, *201*, 117667. [CrossRef]
25. Selvaraju, R.K.; Somaskandan, G. Impact of energy storage units on load frequency control of deregulated power systems. *Energy* **2016**, *97*, 214–228. [CrossRef]
26. Mishra, D.K.; Panigrahi, T.K.; Mohanty, A.; Ray, P.K. Effect of superconducting magnetic energy storage on two agent deregulated power system under open market. *Mater. Today Proc.* **2020**, *21*, 1919–1929. [CrossRef]
27. Sharma, M.; Dhundhara, S.; Arya, Y.; Prakash, S. Frequency stabilization in deregulated energy system using coordinated operation of fuzzy controller and redox flow battery. *Int. J. Energy Res.* **2020**, *45*, 7457–7475. [CrossRef]
28. Mishra, A.K.; Mishra, P.; Mathur, H.D. Enhancing the performance of a deregulated nonlinear integrated power system utilizing a redox flow battery with a self-tuning fractional-order fuzzy controller. *ISA Trans.* **2021**. [CrossRef]
29. Babu, N.R.; Saikia, L.C. Load frequency control of a multi-area system incorporating realistic high-voltage direct current and dish-Stirling solar thermal system models under deregulated scenario. *IET Renew. Power Gener.* **2021**, *15*, 1116–1132. [CrossRef]
30. Kumar, R.; Sharma, V.K. Whale Optimization Controller for Load Frequency Control of a Two-Area Multi-source Deregulated Power System. *Int. J. Fuzzy Syst.* **2020**, *22*, 122–137. [CrossRef]
31. Das, M.K.; Bera, P.; Sarkar, P.P. PID-RLNN controllers for discrete mode LFC of a three-area hydrothermal hybrid distributed generation deregulated power system. *Int. Trans. Electr. Energy Syst.* **2021**, *31*, 1–21. [CrossRef]
32. Das, S.; Saikia, L.C.; Datta, S. Maiden application of TIDN-(1+PI) cascade controller in LFC of a multi-area hydro-thermal system incorporating EV–Archimedes wave energy-geothermal-wind generations under deregulated scenario. *Int. Trans. Electr. Energy Syst.* **2021**, *31*, e12907. [CrossRef]
33. Raj, U.; Shankar, R. Deregulated Automatic Generation Control using Novel Opposition-based Interactive Search Algorithm Cascade Controller Including Distributed Generation and Electric Vehicle. *Iran. J. Sci. Technol. Trans. Electr. Eng.* **2020**, *44*, 1233–1251. [CrossRef]
34. Kumar, A.; Shankar, R. A Quasi Opposition Lion Optimization Algorithm for Deregulated AGC Considering Hybrid Energy Storage System. *J. Electr. Eng. Technol.* **2021**. [CrossRef]
35. Dhiman, G.; Kaur, A. STOA: A bio-inspired based optimization algorithm for industrial engineering problems. *Eng. Appl. Artif. Intell.* **2019**, *82*, 148–174. [CrossRef]
36. Seborg, D.E.; Edgar, T.F.; Mellichamp, D.A.; Doyle, F.J., III. *Process Dynamics and Control*, 4th ed.; Wiley: Seoul, Korea, 2017; ISBN 9781119298489.
37. Mayne, D.Q. Model predictive control: Recent developments and future promise. *Automatica* **2014**, *50*, 2967–2986. [CrossRef]

38. Elshafey, S.; Shehadeh, M.; Bayoumi, A.; Díaz, J.; Pernía, A.M.; Jose-Prieto, M.A.; Abdelmessih, G.Z. Solar thermal power in Egypt. In Proceedings of the 2018 IEEE Industry Applications Society Annual Meeting, IAS 2018, Portland, OR, USA, 23–27 September 2018; pp. 1–8. [CrossRef]
39. Temraz, A.; Rashad, A.; Elweteedy, A.; Elshazly, K. Thermal Analysis of the Iscc Power Plant in Kuraymat, Egypt. *Int. Conf. Appl. Mech. Mech. Eng.* **2018**, *18*, 1–15. [CrossRef]